16.110 Wind Tunnel Lab Report

Peter Sharpe

10/28/19

1 Abstract

The drag on a NACA 0050 body of revolution was estimated using three techniques. The first two techniques were experimental (direct force measurement and wake survey measurement), while the final technique was computational (MTFLOW). The direct force measurement and MTFLOW results were found to be in tight agreement, with only around 10% error averaged across all measurements. Between these two, the MTFLOW results generally predicted higher drag. The wake survey measurements were found to be significantly higher (approximately 60% higher) than the other two measurements.

2 Experiment Setup

2.1 Overview

In this lab, we seek to determine the drag on a NACA 0050 body of revolution of length $l = 10\,\text{in}$. We approach this problem with three methods:

1. Direct force measurement
2. Wake survey measurement
3. Computational modeling

The first two methods described here are experimental in nature. The data analysis procedure for each of these methods is described in the remainder of this document.

2.2 Experimental Apparatus

The experimental apparatus consists of a 1:1 scale model of the body of revolution placed in Building 31's 1.5 x 1.5 ft. open-jet tunnel. The body of revolution is held in place with a small, streamlined strut. This strut consists of a straight extruded NACA 0010 airfoil with a chord $c = 1.25\,\text{in}$. The strut meets the body of revolution in such a way that their trailing edges are coincident. Furthermore, the body of revolution is held exactly in the center of the 1.5 x 1.5 ft. tunnel, which implies that approximately 9" of the extruded strut sees the jet's airflow (assuming the free jet stays collimated). Thus, the exposed planform area of the strut is:

$$S_{strut} = (9\,\text{in}) \cdot (1.25\,\text{in}) = 11.25\,\text{in}^2$$

3 Notes on Uncertainty Propagation

Throughout the data analysis performed in this lab, we seek to propagate an estimate of our experimental uncertainty. Fundamentally, this uncertainty propagation can be expressed in the following manner:

Suppose we have some (generally nonlinear) scalar-valued function f with inputs x_1 through x_n. Then, if σ_f represents the standard deviation of the function's output and σ_{x_i} represents the standard deviation of x_i, the standard deviation of the function's output can be represented (to first order) by:

$$\sigma_f = \sqrt{\left(\frac{\partial f}{\partial x_1}\right)^2 \sigma_{x_1}^2 + \left(\frac{\partial f}{\partial x_2}\right)^2 \sigma_{x_2}^2 + ... + \left(\frac{\partial f}{\partial x_n}\right)^2 \sigma_{x_n}^2} \tag{1}$$

Thus, we can see that there are two key pieces of information that we need in order to propagate uncertainty:

1. The partial derivative of each output (quantity of interest) with respect to each input (data source)
2. The uncertainty (standard deviation) of each data source

These two pieces of information are addressed in the following subsections.

3.1 Partial Derivatives

The first of these pieces of information (the partial derivative of each output with respect to each input) can be computed in a variety of ways.

While it is possible to compute the derivative of each step of the data analysis process by hand and chain-rule through the entire process, this is tedious and error-prone. Numerical differentiation (i.e. finite-differencing) is an option, but it is inelegant, expensive, and imprecise. Symbolic differentiation is exact, but it results in long, tedious formulas that offer little flexibility and opportunity for human insight.

To avoid all this, all analysis for this lab was written to be reverse-mode automatic-differentiation compatible in Python using PyTorch, a popular framework for neural networks and other types of machine learning. In essence, we dynamically track the operations in the analysis while we compute them, building up a computational graph behind the scenes that represents the data flow. Whenever we want to get a gradient of some output with respect to an input, we do a backwards pass through this graph data structure one operator at a time. All operators in the PyTorch library have analytical vector-jacobian products, so propagating backwards through this graph is an efficient, exact, and easy way to get the gradients about some point.

3.2 Uncertainty of Data Sources

The second of these pieces of information (the uncertainty of each data source) is taken from the data itself, and it is noted in this lab report each time a new data source is presented.

Generally, the quantities that we work with here are time-averaged datasets (for example, a voltage averaged over 5 seconds during a given test). Therefore, the most common type of uncertainty that we propagate is the standard deviation of a dataset's mean.

The standard deviation of a dataset's mean can be expressed as follows, assuming a large sample size:

$$\sigma_{\bar{X}} = \frac{1}{\sqrt{n}}\sigma_X \tag{2}$$

where X is the dataset, $\sigma_{\bar{X}}$ is the standard deviation of the dataset's mean, n is the number of samples in the dataset, and σ_X is the standard deviation of the dataset itself. Typically, our datasets are on the order of 5000 samples (5 seconds with 1000 Hz sampling), so results measured in this way result in relatively low uncertainties.

However, it is important that this is a somewhat-incomplete assessment of the error in our dataset: there are other sources of error, like sensor nonlinearity, hysteresis, and drift, that are not considered here. Therefore, the error estimates in this document can really only be considered a *lower* bound on the error in our analyzed data.

4 Ambient Conditions

At the time of measurement the pressure was recorded to be 30.28 inHg (102540. Pa) by `https://www.weather.com`. This was assumed to have a 1-standard-deviation uncertainty of 0.01 inHg.

The temperature was recorded with a thermometer in the wind tunnel room. The recorded temperature was 20.5 C (293.65 K). This was assumed to have a 1-standard-deviation uncertainty of 0.5 K.

Based on this data, viscosity was calculated (using Sutherland's law) and density was calculated (using the ideal gas equation).

5 Preliminary Data Processing

5.1 Data Importing

5.2 Load Cell Calibration

A series of measurements were taken both before and after the experiment in order to establish a relationship between the load cell's voltage and the associated force on the cell.

Two measurements were taken before the lab; one with no weight and another with an 8 oz. weight.

Three measurements were taken after the lab; one with no weight, another with a 2 oz. weight, and a final one with an 8 oz. weight. The new 2 oz. measurement was taken after realizing that most of our recorded forces fell in the extreme lower part of our measurement range; it was assumed that a calibration data point near this range would minimize the effects of sensor nonlinearity.

All measurements were taken for approximately 5 seconds (at 1000 Hz sensor resolution), and all data within a given measurement was time-averaged to give a single mean data point.

The transducer response was assumed to be linear and time-invariant (i.e. no drift). This last assumption was confirmed via inspection; the transducer was found to drift minimally. To further account for any possible drift, the linear fit was calculated as a least-squares fit to all five data points in the calibration sample. This fit is depicted in Figure 1.

6 Direct Force Measurement

The drag force on the body was directly measured with a load cell. Measurements were recorded at speeds of approximately 30, 35, 40, 50, 60, 70, and 73 mph.

Using the following relation (a rewriting of the dynamic pressure equation) in conjunction with dynamic pressure data from the test machine, we can determine the precise speeds of the machine:

$$V_\infty = \sqrt{2q_\infty/\rho_\infty} \tag{3}$$

This results in the speed calculations shown in Table 1.

Run No.	Speed (m/s)	Speed (mph)
1	13.433	30.045
2	15.709	35.140
3	17.838	39.902
4	22.403	50.114
5	26.908	60.193
6	31.401	70.242
7	32.784	73.335

Table 1: Speed Calculations from Dynamic Pressure

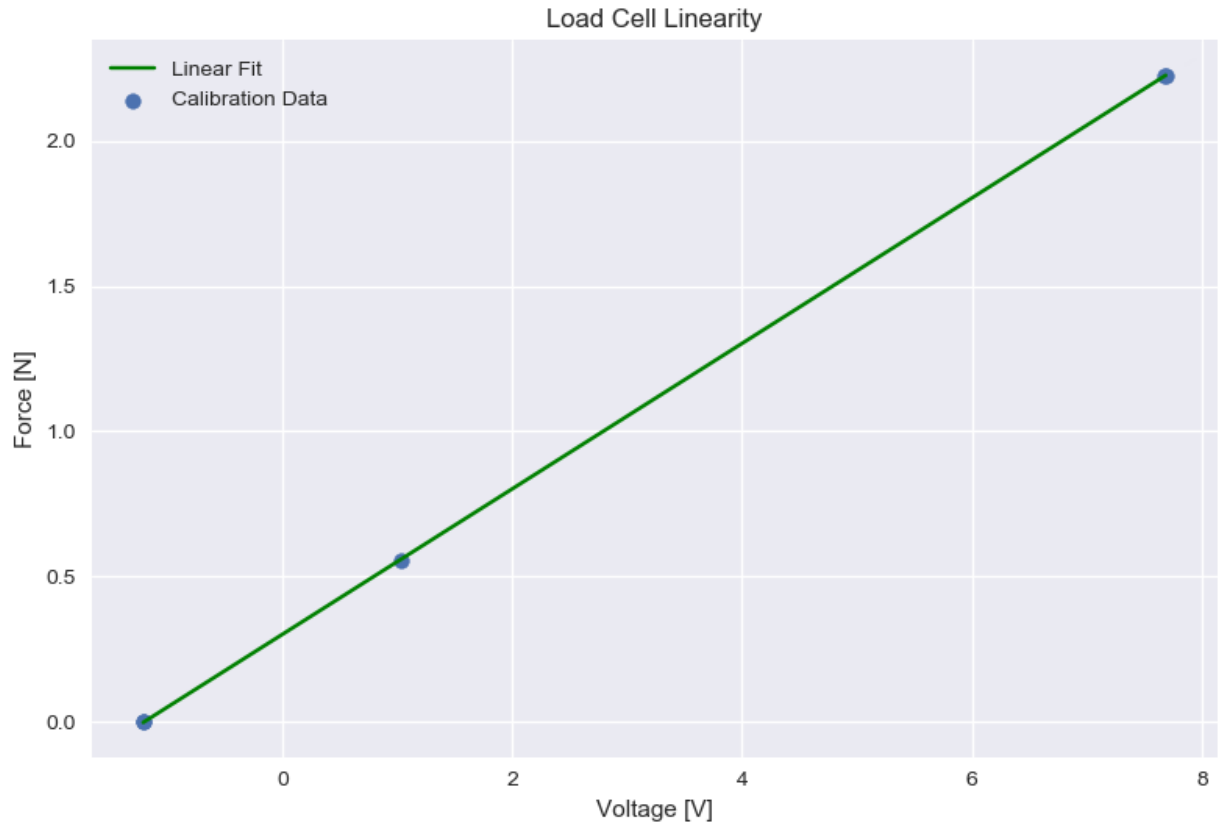

Figure 1: Load Cell Linearity

6.1 Transition Measurements

During this test run, transition measurements were also taken using a portable microphone. These measurements are recorded in Table 2.

Nominal Speed (mph)	Transition x/c
30	0.55
35	0.53
40	0.50
50	0.50
60	0.46
70	0.45
73	0.44

Table 2: Speed vs. Transition Location

6.2 Strut Drag Estimation

In an attempt to isolate the drag of the body from the drag of the strut, we make a computational estimate of the drag of the strut using XFoil.

First, we calculate the Reynolds number at each operating point, now normalized by the strut length (1.25 in). This is given in the second column of Table 3. Then, we obtain the 2D drag coefficient from XFoil; this is given in the third column of Table 3. Finally, we convert these numbers to 3D (by multiplying by the

"span" of the exposed strut, 9") and re-nondimensionalize to the body's frontal area - this is given in the last column of Table 3.

Run No.	$Re_{c,strut}$	$C_D(c_{ref} = c_{strut})$ (2D)	$C_D(S_{ref} = S_{frontal})$ (3D)
1	28579	0.02217	0.0127
2	33421	0.02069	0.0119
3	37950	0.01958	0.0112
4	47662	0.01776	0.0102
5	57249	0.01645	0.0094
6	66807	0.01545	0.0089
7	69748	0.01518	0.0087

Table 3: Strut Drag Calculations (from XFoil)

These numbers are then subtracted from the C_D data measured with the load cell to obtain a more accurate answer for the C_D of the body itself.

6.3 Drag Calculation

Drag is calculated with the following process:

First, the load cell voltages at each speed were converted to force measurements using data from the aforementioned calibration procedure. Then, the force data was converted to C_D by nondimensionalizing to the measured dynamic pressure and reference area (frontal area). Finally, the C_D contribution from the strut was subtracted off. This yielded the results in Table 4.

Reynolds number was calculated by nondimensionalizing based on the speed (calculated from dynamic pressure) and the body's chord.

6.4 Uncertainty Sources

Uncertainty in C_D was assumed to come from two sources: the noise in the load cell's voltage and the noise in the dynamic pressure readings (which would affect C_D nondimensionalization). In both cases, the partial derivative of C_D with respect to each input is calculated by automatic differentiation (as described before). In accordance with the error formula in Equation 1, the errors for both sources were calculated and merged.

Uncertainty in Re was assumed to come from three sources: the noise in the dynamic pressure readings, the ambient temperature (which would affect the viscosity via Sutherland's law and the density via the equation of state), and the ambient pressure (which would affect the density via the equation of state). As before, all of this was calculated using automatic differentiation on our differentiated analysis.

This resulted in the 1-sigma error bounds shown in Table 5. These error bounds have been plotted along with the data in Figure 2, although it is difficult to visualize them as they are quite small compared to the data itself.

Run No.	Re	C_D
1	228633	0.0410
2	267370	0.0358
3	303604	0.0325
4	381301	0.0275
5	457994	0.0240
6	534454	0.0216
7	557987	0.0212

Table 4: Direct Force Measurement Data

Run No.	σ_{Re}	σC_D
1	497	5.44e-6
2	581	5.08e-6
3	660	3.66e-6
4	829	3.01e-6
5	996	2.42e-6
6	1162	2.82e-6
7	1213	2.28e-6

Table 5: Direct Force Measurement One-Sigma Error Bounds

Figure 2: Drag Coefficient: Direct Force Measurement, with error bars

7 Wake Measurement

For the wake measurement survey, a rake of 25 pressure sensors was placed behind the body. This rake measured the dynamic pressure distribution behind the wake (probes 2-24), the edge static pressure (probe 1), and the freestream static pressure (probe 25). These pressures were read off a manometer, as depicted in Figure 3. Here, the familiar wake-defect shape is clearly visible.

7.1 Data Processing

The manometer data is first cleaned and averaged. First, the manometer readings from the +45 and -45 degree runs were averaged together; this is valid because the data should be identical for an axisymmetric flow, and care was taken to ensure that probe 13 was exactly placed on the centerline in both cases (this is clearly shown in Figure 3).

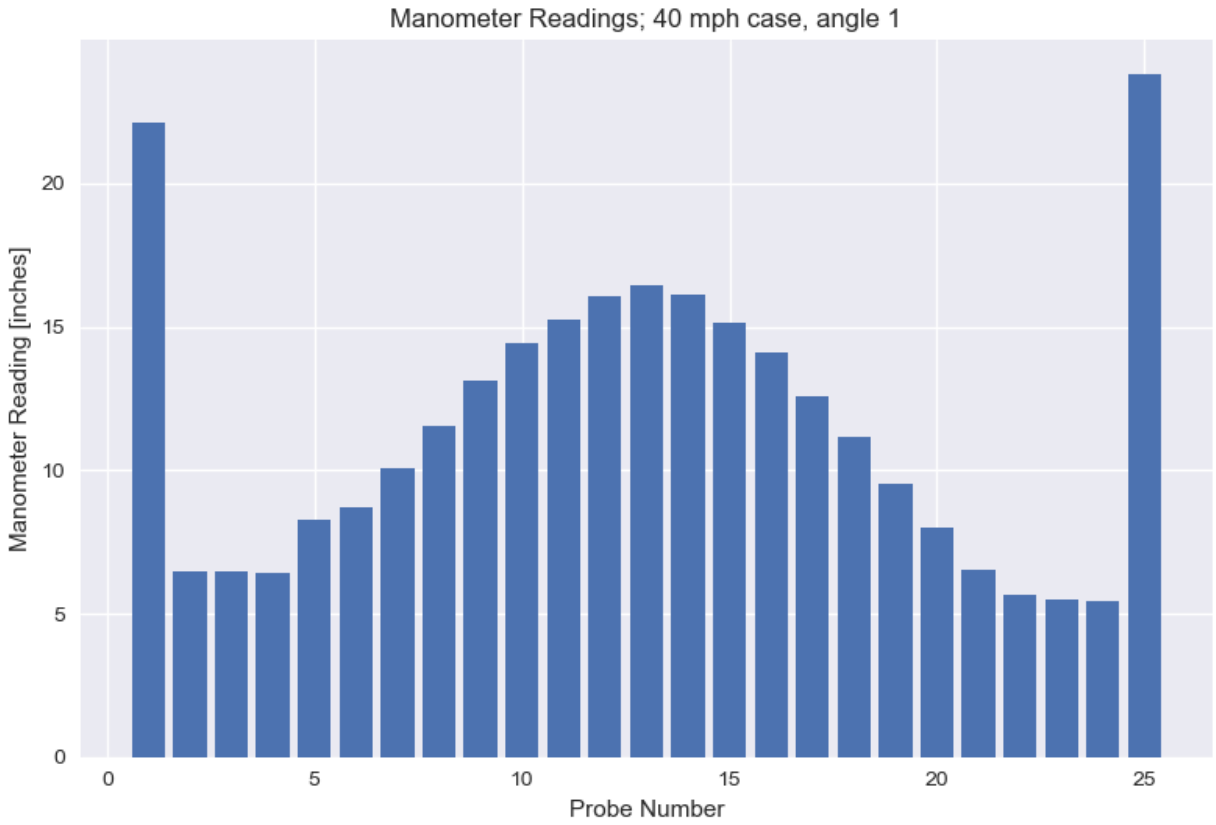

Figure 3: Raw Manometer Readings

Then, this averaged data was further reduced by "folding" the data across itself (i.e. probe 2 was averaged with probe 24, probe 3 was averaged with probe 23, and so on). Once again, because care was taken to ensure that probe 13 was placed exactly on the centerline, this is a valid manipulation of the data. Now, the manometer data for each run was merely a function of radial distance, as it should be for an axisymmetric flow condition. The resulting manometer readout distribution is presented in Figure 4.

Next the ratio of the local velocity to the edge velocity was calculated, using the following formula, taken from the class notes:

$$\frac{u_z}{u_e} = \sqrt{\frac{(p_0(z) - p_{ref}) - (p_e - p_{ref})}{(p_{0_e} - p_{ref}) - (p_e - p_{ref})}} \tag{4}$$

This was used to calculate the momentum defect area Θ and the mass defect area Δ^* using the following relations:

$$\Theta = \int \left(1 - \frac{u}{u_e}\right) \frac{u}{u_e} r dr d\theta \tag{5}$$

$$\Delta^* = \int \left(1 - \frac{u}{u_e}\right) r dr d\theta \tag{6}$$

Under the assumptions of axisymmetry, we can reduce this area integral to a one-dimensional integral (over r). In this case, each "slice" of our integration is an annulus. We may also discretize this integration using our available data. We quickly notice that a simple Riemann-sum-style integration creates an unsatisfying error at $r = 0$: our integrand goes to zero!

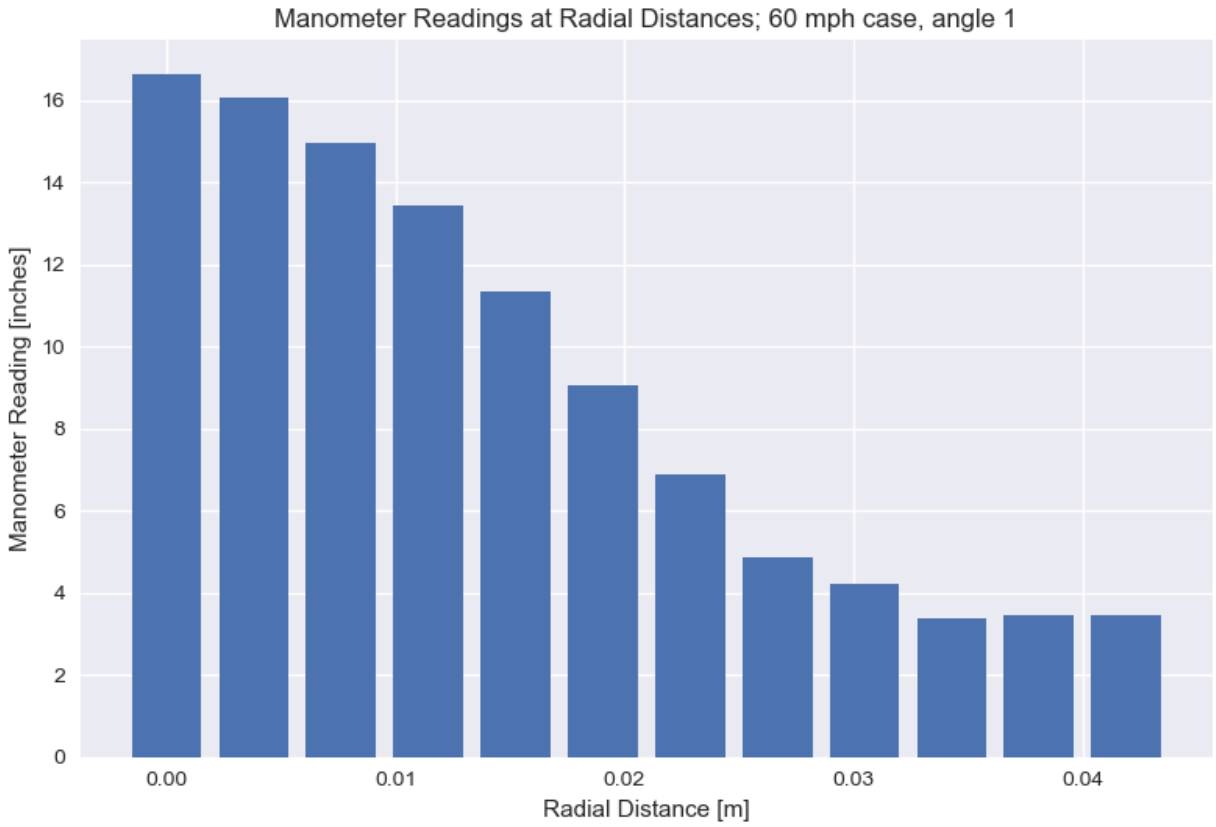

Figure 4: Manometer Readings, Folded

Moving to higher-order interpolation schemes (like trapezoidal integration) does not fix this; however, we can fix this by limiting our Riemann-style integration to the velocity values and using exact ring area calculations for the integration area. This results in nonzero integrand influence of the center node, and we are once again satisfied.

The boundary layer shape factor at the rake location H_x can be found as the ratio between the local momentum defect and the local mass defect. H was calculated to be approximately 1.29 for the 40 mph case and 1.32 for the 60 mph case. This is somewhat lower than expected (typical values for turbulent boundary layers are around 1.6), but we note that this measurement is a) in the wake, where H is asymptotically dropping to 1 and b) in an axisymmetric case, while most of our intuition comes from planar 2D theory.

We next use the Squire-Young correction factor to propagate Θ into the Trefftz plane. For this, we need to know the ratio of the edge velocity to the freestream velocity; this can be conveniently found with the following relation:

$$\frac{u_e}{V_\infty} = \sqrt{\frac{(p_{0_e} - p_{ref}) - (p_e - p_{ref})}{(p_\infty - p_{ref}) - (p_e - p_{ref}}} \tag{7}$$

Using this equation, we obtain values for u_e/V_∞ that are on the order of 0.93 for both the 40 mph and 60 mph case. With this information, we may now use the Squire-Young correction:

$$\Theta_\infty = \Theta_x * \left(\frac{u_e}{V_\infty}\right)^{\frac{H_x+5}{2}} \tag{8}$$

With this, we obtain estimates for Θ_∞ of 3.35e-4 m^2 for the 40 mph case and 2.64e-4 m^2 for the 60 mph case. We may finally convert this into a profile drag coefficient using the following relation, again taken from

the class notes:

$$C_D = 2\frac{\Theta_\infty}{S_{ref}} \tag{9}$$

Thus we calculate that $C_D = 0.0529$ for the 40 mph case and $C_D = 0.0417$ for the 60 mph case.

Associated Reynolds numbers may also be computed; this procedure is detailed in the previous direct force measurement section and will not be repeated. The Reynolds numbers are 305805 for the 40 mph case and 456192 for the 60 mph case.

These results are shown in Figure 5.

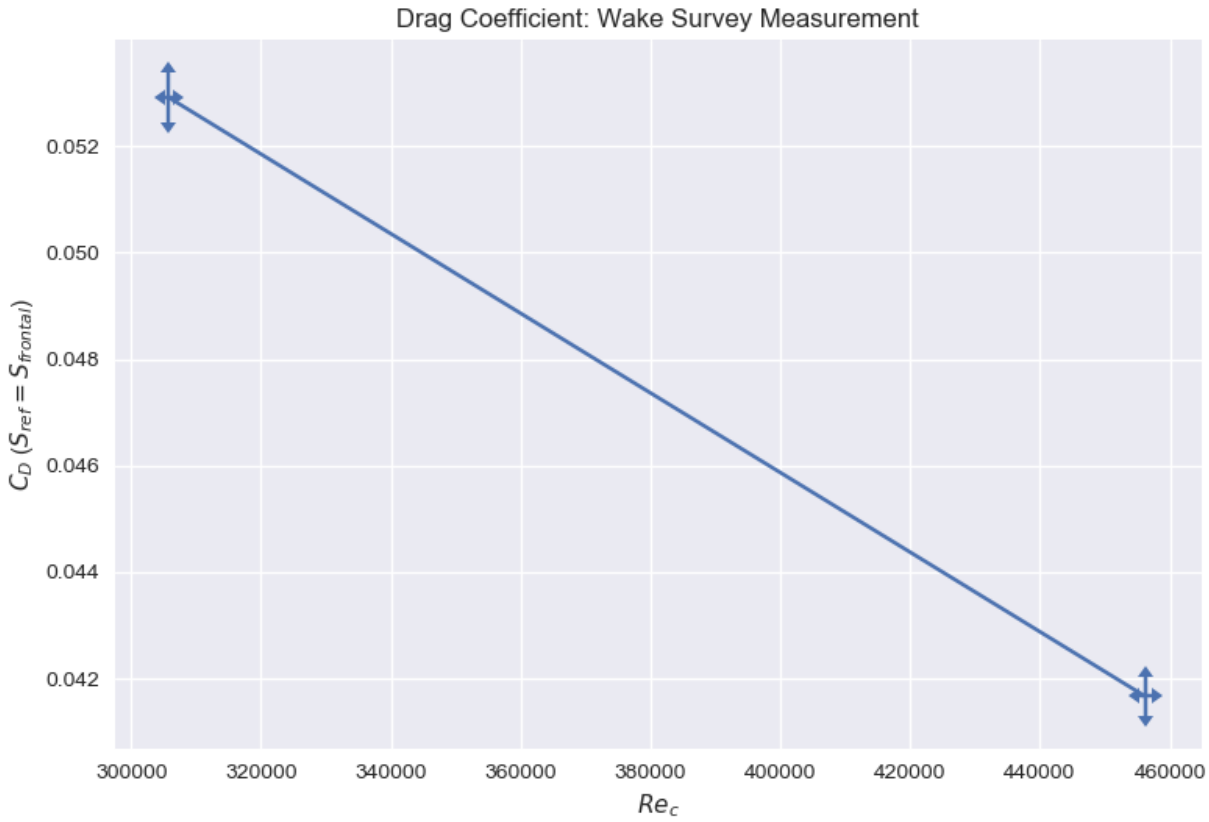

Figure 5: Wake Survey Measurement

7.2 Uncertainty Sources

Uncertainty in C_D was assumed to come from one source: the manometer reading. Here, the one-sigma uncertainty in the reading was assumed to be 0.05", or half a tick mark.

Uncertainty in Re was assumed to come from two sources: the ambient temperature (which would affect the viscosity via Sutherland's law and the density via the equation of state), and the ambient pressure (which would affect the density via the equation of state).

Once again, all of the partial derivatives required were calculated using automatic differentiation. These result 1-sigma error bounds have been plotted along with the data in Figure 5.

7.3 Requested Plots and Data

The requested plots of u/u_e versus r/R_{max} have been provided in Figures 6 and 7. The tabulated data requested is listed in Table 6.

Figure 6: Wake Velocity Profile, 40 mph

Case	Δ^* [m^2]	Θ_x [m^2]	u_e/V_∞	H	Θ_∞ [m^2]
40 mph	5.23e-4	4.06e-4	0.941	1.290	3.35e-4
60 mph	4.41e-4	3.35e-4	0.927	1.317	2.64e-4

Table 6: Computed Values

8 Computational Modeling

The axisymmetric flow solver MTFLOW was used to estimate the drag on the body computationally. Sweeps were run from $Re = 200000$ to $Re = 600000$ to approximately match the range tested experimentally. One of the unknown parameters in the formulation of the computational model was N_{crit}, the critical amplification factor used in the e^N wave-growth transition prediction model. Sensible guesses of 4 and 9 were made (based on qualitative assessments of the wind tunnel), with the assumption that the true value would likely lie somewhere within this range. Results of this calculation are shown alongside the other methods in Figure 8.

9 Overlay of All Methods

All methods (direct force measurement, wake survey measurement, and computation) are combined to yield the plot in Figure 8.

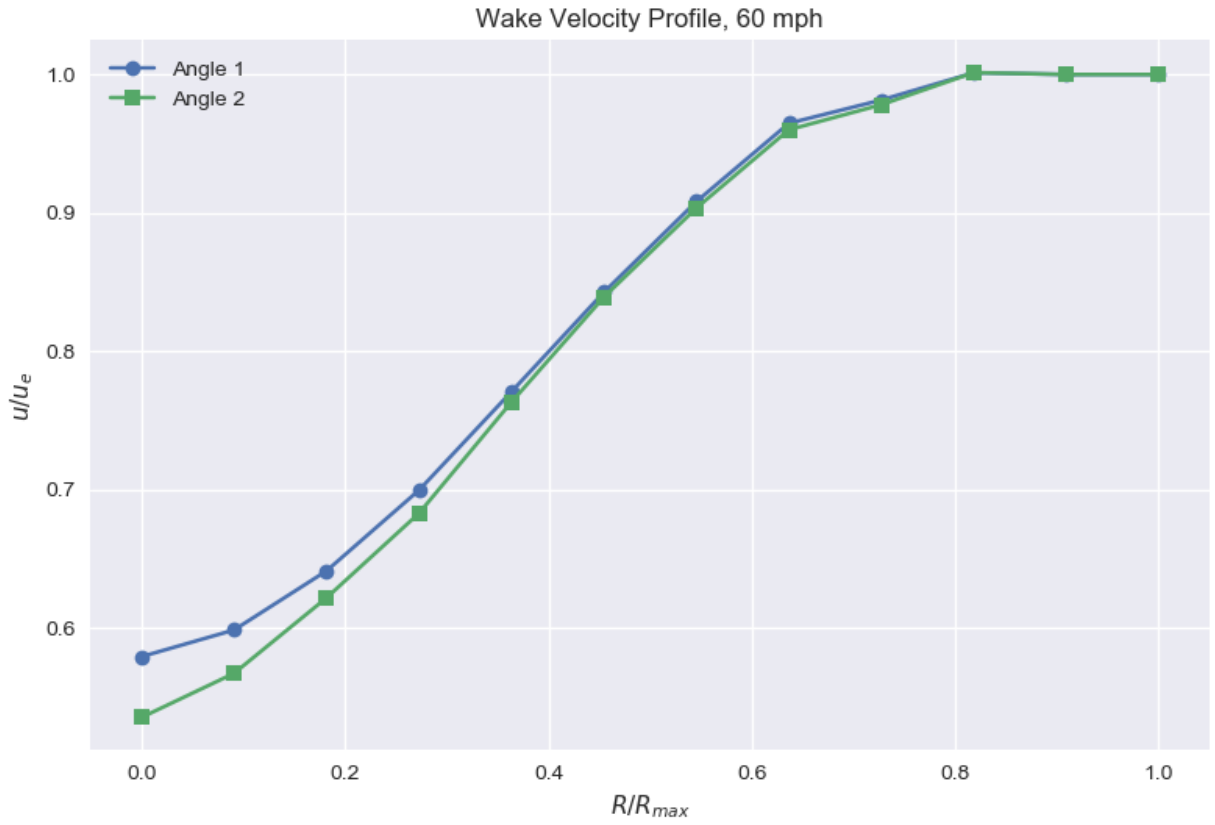

Figure 7: Wake Velocity Profile, 60 mph

10 Reproducibility

All raw data and analysis code for this lab (including the automatic-differentiated uncertainty quantification) is available online at: `https://github.com/peterdsharpe/16110-Wind-Tunnel-Lab`.

11 Conclusion

The drag on a NACA 0050 body of revolution was estimated using three techniques. The direct force measurement and MTFLOW results were found to be in tight agreement, with only around 10% error averaged across all measurements. Between these two, the MTFLOW results generally predicted higher drag. The wake survey measurements were found to be significantly higher (approximately 60% higher) than the other two measurements.

Uncertainty quantification was performed to some extent using error propagation methods. However, there are many sources of error that were not accounted for that could serve to explain the discrepancies in our results. In the direct force measurement, we implicitly made the assumption that the load cell had a linear voltage response, and we neglected to propagate error through the load cell slope and offset due to the difficulty of differentiating a least-squares fit. In the wake survey measurement, we qualitatively noticed during the lab that the manometer levels appeared to fluctuate by small amounts; this would imply that our true measurement uncertainty is higher than simply a single tick mark. In the computational modeling, we made sensible guesses for Ncrit, but these were not experimentally validated (and going beyond that, we make assumptions about the validity of e^N transition modeling, TSL assumptions, discretization assumptions, and more). Thus, the discrepancies we recorded were not totally unexpected.

This does underscore two key takeaways, though:

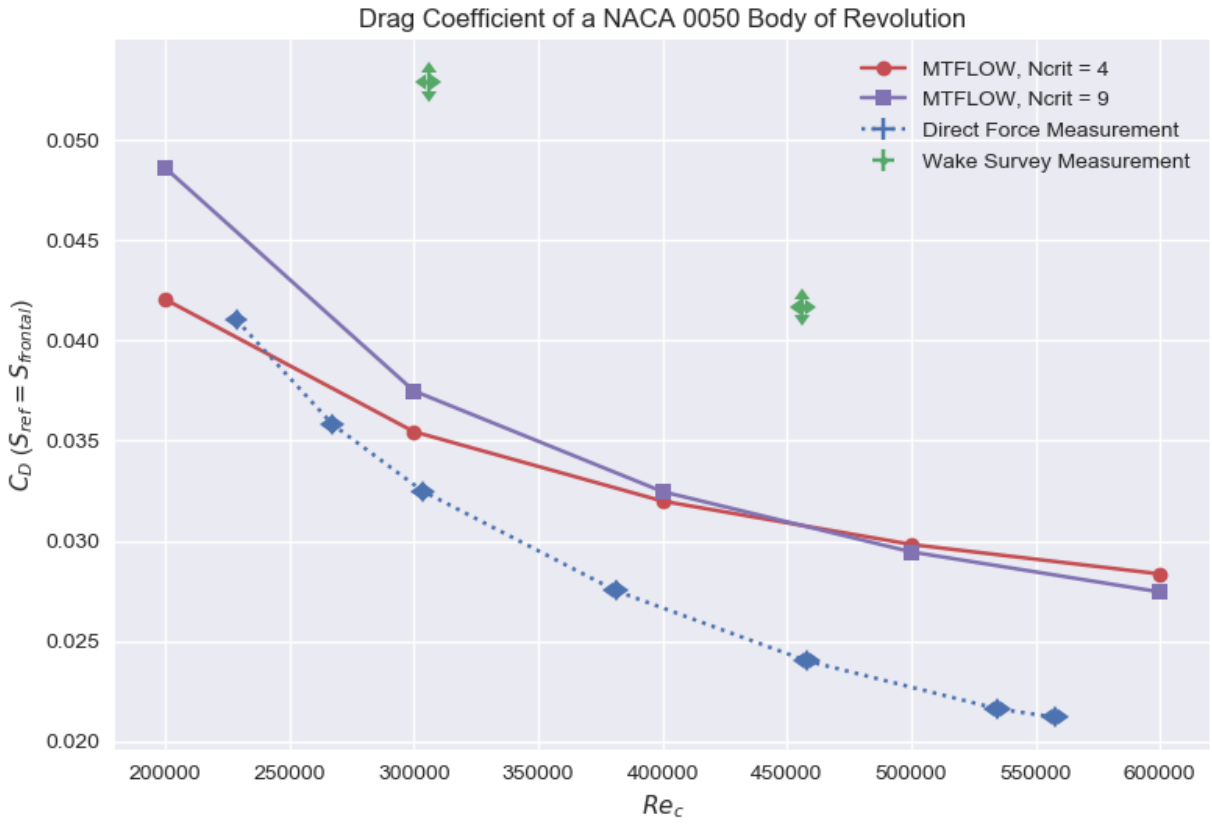

Figure 8: Combined Plot

1. Drag is quite difficult to determine experimentally
2. Assuming that the true drag values lie somewhere in the middle of all three data series, computational methods can be at least as good at predicting drag as lab experiment (with the qualifications that this statement is based on just one experiment that only measured attached, non-lifting flow on a relatively-simple body of revolution).